Journal Name

ARTICLE

Plasma Modification of the Electronic and Magnetic Properties of Vertically Aligned bi-/tri- layered Graphene Nanoflakes

Received 00th January 20xx,
Accepted 00th January 20xx

DOI: 10.1039/x0xx00000x

www.rsc.org/

Sekhar C. Ray,[a,*] Navneet Soin,[b,c] Way-Faung Pong,[d] Susanta S. Roy,[e] André M. Strydom,[f] James A. McLaughlin[c] and Pagona Papakonstantinou[c]

Saturation magnetization (M_S) of pristine bi-/tri-layered graphene (denoted as - FLG) is enhanced by over four (4) and thirty-four (34) times to 13.94 x 10^{-4} and 118.62 x 10^{-4}emu/gm, respectively, as compared to pristine FLGs (M_S of 3.47 x 10^{-4}emu/gm), *via* plasma-based-hydrogenation (known as Graphone) and nitrogenation (known as N-graphene) reactions, respectively. However, upon organo-silane treatment on FLG (known as Siliphene), the saturation magnetization is reduced by over thirty (30) times to 0.11 x 10^{-4} emu/gm, as compared to pristine FLG. Synchroton based X-ray absorption near edge structure spectroscopy measurements have been carried out to investigate the electronic structure and the underlying mechanism responsible for the variation of magnetic properties. For graphone, the free spin available *via* the conversion of $sp^2 \rightarrow sp^3$ hybridized structure and the possibility of unpaired electrons from induced defects are the likely mechanism for ferromagnetic ordering. During nitrogenation, the Fermi level of FLGs is shifted upwards due to formation of graphitic like extra π-electron that makes the structure electron-rich, thereby, enhancing the magnetic coupling between magnetic moments. On the other hand, during the formation of siliphene, substitution of C-atom in FLG by Si-atom occurs relaxes out the graphene plane to form Si-C tetrahedral sp^3-bonding with non-magnetic atomic arrangement showing no spin polarization phenomena and thereby reducing the magnetization. Thus, plasma functionalization offers a simple yet facile route to control the magnetic properties of the graphene systems and has potential implications for spintronic applications.

Introduction

Graphene is a single atomic layer of sp^2 hybridized carbon atoms covalently bonded to three other atoms arranged in a honeycomb lattice with a thickness of only 0.34 nm.[1-7] Its unique structural, mechanical and electrical properties with high carrier mobility make it one of the most important topics in advanced materials science of the present era.[8-14] Due to its unique properties, a variety of applications have been proposed and indeed reported in the literature including chemical sensors[15, 16], nano-electronics devices[17], hydrogen storage systems[18] and polymer nano-composites[19]. Especially, graphene-based spintronics and magnetic materials are envisaged to be highly promising due to its extraordinary carrier mobility and may provide an easy way to integrate spin and molecular electronics.[1] The long spin diffusion length of graphene makes it highly attractive for spintronic devices and has triggered a quest for integrating the charge and spin degrees of freedom.[1] However, graphene is intrinsically non-magnetic and lacks localized magnetic moment due to the delocalized π-bonding network, which limits its applications in spintronic devices.[20] Therefore, synthesis of ferromagnetic graphene or its derivatives with high magnetization is necessary for spintronics applications. For the synthesis of ferromagnetic graphene, dopants like hydrogen, nitrogen, boron, silicon, sulphur, selenium and/or different transitions metals have been explored with varying degrees of success.

One important development since the discovery of graphene has been the discovery of the so-called graphone and graphane, which are partially/fully hydrogenated forms of graphene and were first theoretically reported by Zhou et al.[21] and Lu et al.[22], respectively. In graphone/graphane form, the carbon atoms are sp^3 hybridized making them particularly suitable for spintronic applications. The predicted graphone/graphane structures were later confirmed experimentally by Ray et al.[23] and Elias et al.[24] by exposing graphene to hydrogen plasma (ranging from a few minutes to several hours) and it was observed that the magnetic moment of plasma functionalised graphene is enhanced dramatically.

[a.] *Department of Physics, College of Science, Engineering and Technology, University of South Africa, Private Bag X6, Florida, 1710, Science Campus, Christiaan de Wet and Pioneer Avenue, Florida Park, Johannesburg, South Africa.*
[b.] *Institute for Materials Research and Innovation (IMRI), University of Bolton, Deane Road, Bolton, BL3 5AB, United Kingdom.*
[c.] *Nanotechnology and Integrated Bioengineering Center (NIBEC), School of Engineering, University of Ulster, Jordanstown campus, Newtownabbey, BT37 0QB, United Kingdom.*
[d.] *Department of Physics, Tamkang University, Tamsui 251, Taipei, Taiwan.*
[e.] *Department of Physics, School of Natural Sciences, Shiv Nadar University, Gautam Budh Nagar 203207, UP, India.*
[f.] *Highly correlated matter research group, Department of Physics, University of Johannesburg, Auckland Park 2006, South Africa.*
Electronic Supplementary Information (ESI) available: See DOI: 10.1039/x0xx00000x

Graphane is predicted to have a stable structure with a band gap of 3.5 eV, consisting of a graphene layer in which each of the C atom is sp^3-bonded to one H atom above and below in an alternating manner[25]; whereas graphone (one sided hydrogenation of graphene) has sp^3 bonding of C with H on only one side of the graphene and is useful in electrical isolation for graphene-based circuits.[26] The nitrogen-doping and/or N-functionalization of graphene has also been shown as an effective route to obtain high magnetization values owing to its comparable atomic size to carbon and the presence of five valence bonds with carbon atoms[27], which can introduce magnetic moment into graphene[28]. Theoretical studies too have confirmed that the N-doping is an effective method to introduce magnetic moments into graphene.[28-32] These localized magnetic moments can be induced by different arrangement of N atoms with the pyridine and pyrrole like N-doping defects breaking the degeneracy of the spin polarisation of graphene.[28-32] Indeed, Liu et al.[33] have observed high values of magnetization in ferromagnetic graphene oxide (GO), when doped with nitrogen. Post N-doping, the Fermi level shifts upwards due to presence of extra π-electrons which makes graphene electron-rich[34] thereby enhancing the coupling *via* the reduction of the magnetic moment distance.[33] Zhang et al.[31] proposed that the combination of vacancy defects and N atoms may provide a unique way for enhancing the magnetic moment of graphene. The silicon atoms, which are introduced into the graphene structure as heteroatoms, can also tune the magnetic and electronic properties of graphene[35]. Needless to say, the implementation of Si-doping in graphene requires a clear understanding of the effect of silicon atoms on graphene for the fabrication of various electronic and magnetic devices. It was experimentally observed by Pao et al.[35] that threefold-coordinated Si in graphene results in sp^3 hybridization. Besides, a single Si-impurity in monolayer graphene and Si-doped bilayer-graphene have also been investigated, which shows existence of covalent bonding between the Si atoms of different layers.[36] This stable linked structure strongly suggests the importance of interaction between Si-impurity atoms in graphene. However, unlike the hydrogen and nitrogen doping of graphene, there are only a handful of experimental studies on the electronic and magnetic properties of Si-doped/functionalized graphene. Particularly, there are no reported studies on the magnetic properties of Si-doped graphene, so it is necessary and requires exploring these properties on this derivative graphene material (*Si-doped graphene*) for practical application as a diluted magnetic semiconductor (DMSs) in spintronics.[37]

In our earlier work, we had reported on the synthesis of hydrogen-functionalized graphene (referred as graphone/graphane) on graphene layer (referred as graphene supported graphone/graphane bi-layer nano-structure materials) and found that the magnetic moment is enhanced significantly with potential implications for their use in spintronic applications.[23] We also reported that the GO shows higher ferromagnetism than reduced graphene oxide (rGO), and the origin of ferromagnetism was identified as the C-2*p*(σ*)-derived states that involve defects/vacancies rather than C-2*p*(*π**) states that are bound with oxygen-containing and hydroxyl groups on GO-sheets; which could also be use in spintronic applications.[38] In the present study, we have further investigated the significant enhancement of magnetic properties of FLGs upon doping by nitrogen plasma (referred as N-Graphene). We have also studied the magnetic effect of organo-silane-treated (Si-doped/functionalized) graphene (referred as Siliphene) and compared with Graphone and N-Graphene for the possibility of use in spintronic applications. The magnetic properties were studied by a superconducting quantum interference device (SQUID)-type magnetometer and magnetic force microscopy (MFM) measurements. The electronic structure and microstructural properties were correlated with magnetic properties using a variety of techniques including X-ray Absorption near Edge Structure (XANES), X-ray Photoelectron Spectroscopy (XPS), Raman spectroscopy and field emission analysis among others.

Experimental

Preparation of few layer graphene (FLG), Graphone, N-Graphene and Siliphene

The synthesis of FLG was carried out in a SEKI microwave plasma enhanced chemical vapor deposition system, equipped with a 1.5 kW, 2.45 GHz microwave source. The substrates used were bare n-type heavily doped Si wafers (resistivity < 0.005 Ω.cm) (10 mm x 10 mm). Prior to growth, the substrates were pre-treated with N_2 plasma at 650 W at 40 Torr while the substrate temperature was maintained at 900^0C. Synthesis was then carried out using CH_4/N_2 (gas flow ratio=1:4) plasma at 800 W for a duration of 60 s. The FLG were allowed to cool under a constant N_2 flow. The conditions used were similar to the ones reported in our previous publications.[48, 49, 88-90] The hydrogen microwave plasma treatment of the FLG was carried out at substrate temperatures of 50^0C (referred as graphone) at a chamber pressure of ~2 Torr with a treatment time of 90 s and microwave power of 150 W.[23] Nitrogen doping/functionalization of FLG (referred as N-graphene) was carried out using an Electron Cyclotron Resonance (ECR) nitrogen plasma treatment for 5 min[48]; whereas Si is doped/functionalized (referred as siliphene) using RF-plasma glow discharge process with specific Ar/tetra-methyl-silane [TMS, $Si(CH_3)_4$] ratio at room temperature for 5 min.[35]

Material Characterization

Raman spectroscopy was performed using an ISA LabRam system equipped with a 632.8 nm He-Ne laser with a spot size of approximately 2-3 mm, yielding a spectral resolution of better than 2 cm^{-1}. Due care was given to minimize sample heating by using a low laser power below 2 mW. The XPS spectrum was measured on a Kratos Axis Supra DLD employing an Al *K*α radiation (1486.6 eV). The X-ray absorption near edge structure (XANES) spectra was obtained using the high-energy spherical grating monochromator 20A-beamline at the National Synchrotron Radiation Research Center (NSRRC), Hsinchu, Taiwan. The magnetic properties of these FLGs were

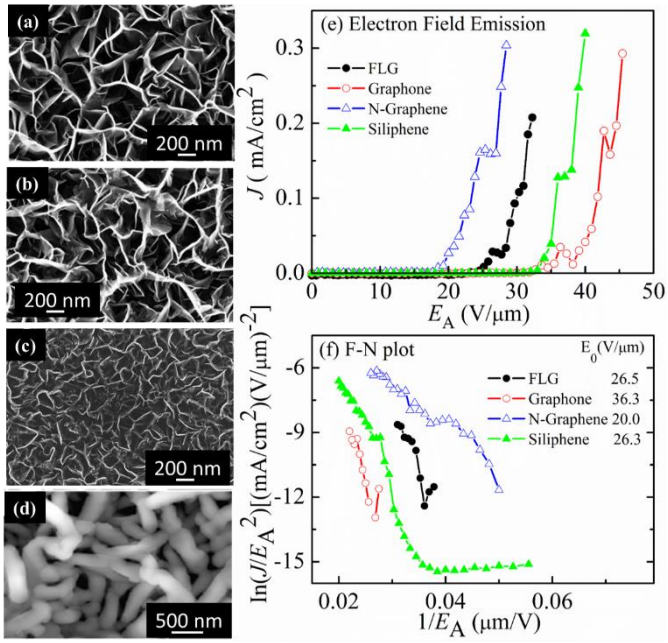

Figure 1: SEM images of (a) pristine FLGs, (b) Graphone, (c) N-graphene and (d) Siliphene. The (e) electron field emission behaviour showing current density (*J*) as a function of applied electric field (E_A) and (f) Fowler-Nordheim plot obtained from EFE measurements. (a, b) Reproduced from S. C. Ray et al., *Sci. Rep.*, 2014, **4**, 3862.

characterized by a SQUID-type magnetometer with sensitivity better than 5 x 10^{-8} emu. The topographical and magnetic force microscopy (MFM) measurements were carried out using a Veeco Dimension 3100 AFM connected to a Nanoscope IIIa controller in the tapping mode configuration. To detect magnetic domains in the prepared samples, low moment magnetic probes with Co/Cr coatings were used. In addition, the electron field emission (EFE) was measured using a Keithley source meter.

Results and discussion

The scanning electron microscopy (SEM) images of all the FLG samples are shown in Fig. 1(a-d) respectively. It is evident that the as-synthesized, pristine FLGs are vertically aligned to the underlying Si substrate and are randomly intercalated with each other to form a porous mesh-like network [23]. The post-growth H_2 and N_2 plasma treatment processes does not disturb the vertically aligned nature of the graphene platelets; however, the plasma treatment does lead to an increase in the number of sharp graphene edges throughout the graphone and N-graphene samples. It is also found that the apparent thickness of the edges of graphene platelets is reduced due to plasma etching effects as reported in our previous work [23]. However, for organo-silane-treated FLGs (siliphene), a significant increase in the thickness of FLG *via* the formation of round-shaped, rod- and tube-like structures was observed in the SEM image (Figure 1(d)). Figure 1(e) shows the plot for EFE current density (*J*) as a function of the applied electric field (E_A) for graphene, graphone, N-graphene and siliphene. The figure shows the existence of a classical threshold electric field at which the current density, *J* increases significantly from a zero value. As compared to pristine FLGs, the threshold electric field is reduced for N-graphene whereas for graphone and siliphene, the threshold value increases, which suggests that the H and Si treatment increases the activation energy whereas the N treatment reduces the activation energy. The Fowler-Nordheim (F-N) plots shown in Fig. 1(f) clearly show the existence of threshold electric field or turn-on electric field (E_{TOE}) which was measured by linear fitting of the curve in the high electric field region. For pristine FLGs, the E_{TOE} value were 26.5 V/μm, which was further increased to 29.3 (36.5) V/μm for graphone(siliphene) by the increase in the sp^3-hybridized bonds in graphone/siliphine.[23, 35, 39] In the case of N-graphene, the E_{TOE} decreases to 20.0 V/μm due to the increase in the number of defect sites, lowering of the Fermi level and the possible enhancement of the sp^2 bonding, as observed by Chiou et al.[40] in nitrogen functionalized graphene nanoflakes. In the case of H and Si functionalised FLGs, the strong preference for sp^3 bonding has been argued to be related to the outward relaxation of the H and Si atoms.[23, 35, 39] The sp^2 hybridised bonds as well as the upwards movement of the Fermi level in the N-graphene network are responsible for the enhancement of electron field emission current whereas the H, Si doping induced sp^3 bonding configuration leads to the reduction of field emission current due to the reduction in the metallic character. Therefore, reduction of the EFE current in graphone/siliphene is due to the decrease of the number of sp^2 hybridized bonds in the network which are responsible for the metallic EFE current.[41, 42] These results clearly indicate that H- and Si- doping promote the three-dimensional sp^3 bonding configuration; whereas N-doping promotes sp^2 bonding configuration.[41, 42]

Raman Spectroscopy Figure 2 shows the deconvoluted Raman spectra of pristine FLGs along with graphone, N-graphene and siliphene in the range of 1200 – 3000 cm^{-1}, obtained using a laser excitation of wavelength 632.8 nm. The main Raman spectra features of carbon-based materials are the G and D bands that lie around 1580 and 1350 cm^{-1}, respectively. While, the G band corresponds to optical E_{2g} phonons at the Brillouin zone centre; the D peak arises due to the breathing-like modes (corresponding to TO phonons close to the K point) and requires a defect for its activation via an inter-valley double resonance Raman process. Moreover, the intensity of the D-peak provides a simple measure of the amount of disorder in graphene and graphene based structures. The overtone, 2D band appears at around 2680cm^{-1}, being the sum of two phonons with opposite momentum, acts as a fingerprint for monolayer graphene and is present even in the absence of any defects.[43-47] The D` peak observed at ~1620 cm^{-1}, occurs via an intra-valley double resonance process in the presence of defects. Since the D band requires a defect to be Raman active, it is generally not used to characterize doping. However, both the G and 2D bands are both strongly influenced by the carrier concentration and they have been extensively studied for doping characterization.[43-47] Detailed

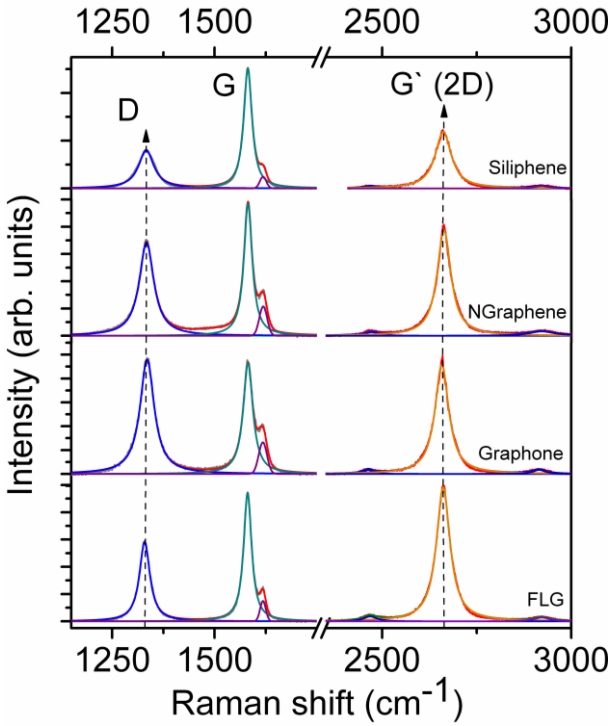

Figure2. Raman spectra of pristine and functionalised FLG samples, (b) the changes occurring in the peak position of G and 2D band.

analysis of band shape analysis of the Raman bands was carried out by undertaking analysis of the band shape and full width at half-maximum (FWHM) parameters by fitting the first and second order Raman spectra using Lorentzian peak shapes for the D, G, and G`(2D) bands, and Gaussian peak for the D` band. This is in accordance with our previous studies carried out on few layered graphene systems.[23, 48, 49] As compared to the peak position (1580.5 cm^{-1}) and the FWHM (23.4 cm^{-1}) of the G band in pristine FLGs; upon nitrogen doping, the G band upshifted slightly to 1581.5 cm^{-1} with a corresponding increase in FWHM to 24.5 cm^{-1}. It should be noted that although the G band peak shifts are more prominent in electrostatically gated monolayered graphene, nevertheless, similar stiffening of the G band along with FWHM enhancement has been previously observed in chemically doped graphene.[48, 50, 51] This blue shift of the G band (E_{2g} mode at Γ) along with the associated broadening of FWHM has been attributed to the nonadiabatic removal of the Kohn anomaly from the Brillouin zone center, Γ.[48, 50, 51] The electron-cyclotron resonance plasma treatment induces the substitution of electron-donating nitrogen atoms into the graphene lattice, with the overall effect of a rise in the Fermi level that is then observed in the blue shift of the G band in Raman spectra.[48] The incorporation of N into the FLG structure may generate C–N and N–N bonds at the expense of the C–C bonds. However, the C–N vibration modes, which lie between the G and D bands, cannot be identified owing to the insensitivity of Raman excitation to distinguish between the cross sections of C and N atoms. In electric field gated graphene, by applying suitable bias, both electron and hole conduction mechanisms are accessible by shifting the Fermi level and can be observed in the upshift of the G peak in the Raman spectra for both the cases.[51] Similarly, the G`(2D) band shows an upshift from 2661.4 cm^{-1} to 2663.1 cm^{-1}, with a slight increase in the FWHM from 43.7 cm^{-1} to 44.3 cm^{-1}. This blue shift of the 2D band has also been observed by Yan et al., and has been attributed to the increased disorder and reduction in the crystallinity in N-doped graphene and is consistent with those observed in electrostatically gated graphene.[51, 52] An I_{2D}/I_G ratio of >1 is indicative of the formation of bi-layer/tri-layer graphene, whereas an I_{2D}/I_G ratio of <1 represents tri- or multi-layered graphene.[53, 54] It is also observed that the G-band shifts on hydrogenation and organo-silane treatment too which is caused by a change in charge density[55] and moves the Fermi level of FLG. Correspondingly, upon hydrogenation, the G band downshifted to 1579.1 cm^{-1} with a lowering of FWHM to 21.5 cm^{-1}. When hydrogenated, the graphone samples are expected to be electron doped as carbon is slightly more electronegative than hydrogen and is corroborated by the red shift observed in the G band position.[55] The G`(2D) spectra of graphone samples shows a significant downshift from 2661.4 cm^{-1} to 2657.9 cm^{-1} with a slight broadening of the line width from 43.7 cm^{-1} to 44.4 cm^{-1}. This is accompanied by the change in the I_D/I_G (I_{2D}/I_G ratio) ratio to 0.32 (1.03) from 0.83 (1.02) for pristine FLGs, and as mentioned earlier signifies the formation of bi/tri-layered graphene. A similar reduction in the graphene layers upon plasma hydrogenation process has been observed previously as well and is corroborated by both the values of I_{2D}/I_G and the FWHM of the 2D band.[56] In the recent study carried out by Eckmann et al., the ratio of D and D` bands was used to comment upon the nature of defects induced in graphene through fluorination and $Ar^+$ bombardment.[57] In their study it was observed that the $I_D/I_{D`}$ ratio was maximum (~13) for sp^3 type defects and reaches a minimum (~3.5) for boundaries in graphite.[57] In our study, the $I_D/I_{D`}$ ratio varied from 3.03 for pristine FLGs vs. 3.23 for FLG:N and 5.5 for the FLG:H samples. The rather high value of $I_D/I_{D`}$ for the pristine samples can be attributed to the finite crystallite size and hence the presence of boundaries, the combination of which leads to the defect induced D peak as well. While both the N-Graphene and Graphone samples were prepared using plasma modification, the differences in the working pressures as well as the power leads to significant differences in the formation of defects. For graphone samples, the increase in the $I_D/I_{D`}$ ratio can be attributed to the formation of sp^3 bonds as well as the vacancy-like defects produced due to H^+ bombardment in the microwave plasma.[23] While the N^+ ion bombardment too will produce substitutional and vacancy-like defects in the graphene lattice, the electron-cyclotron resonance conditions used for functionalisation limits the amount of defects produced in the graphene lattice due to the lower ion energy of the species.[48] Similarly, upon organo-silane treatment, the $I_D/I_{D`}$ ratio increased to 3.30 from 3.03 for pristine FLGs which again can be attributed to the formation of sp^3 type defects and structures for FLG:Si samples. From the Raman spectrum of siliphene, it can be observed that there are no significant SiC segregations or clusters in siliphene. As compared to pristine FLGs, both the D and G bands for siliphene are upshifted to

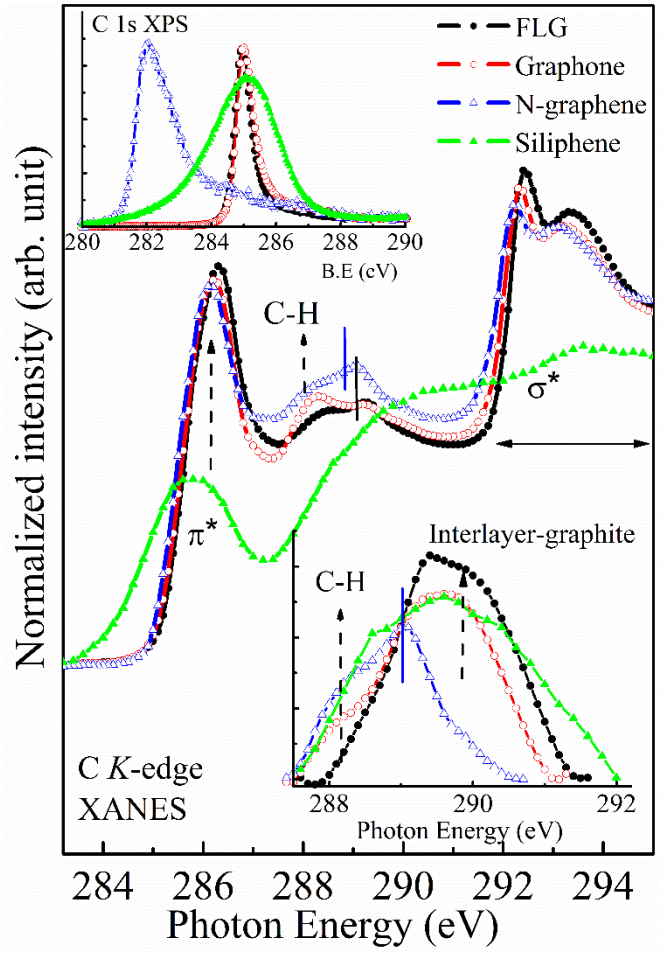

Figure 3. C *K*-edge XANES spectra of the pristine and plasma functionalised FLGs with the lower inset showing the signatures of C-H bonds and interlayer graphite states. The inset above shows the changes in the C1s core level XPS spectra.

1333.0 and 1581.3 cm^{-1}, respectively accompanied by the broadening of D (45.1 cm^{-1} from 30.7 cm^{-1} for pristine FLG) and G bands (24.4 cm^{-1} from 23.4 cm^{-1} for pristine FLG). This broadening of the bands can be attributed to the formation of large number of sp^3-hybridized atoms in siliphene after the weakening of the C-C bond caused due to bonding with the Si-atom. The consequential reduction of the I_D/I_G ratio (a sp^2/sp^3 signature) upon functionalization with Si [FLG:0.80→siliphene:0.39] also indicates the formation of large number of sp^3-hybridized atoms *via* a partial conversion of the sp^2 bonding, which is a mixture of single and double C-C bonds, to the sp^3 bonding with only single C-C bonds. The G`(2D) band for siliphene samples does not show any appreciable movement, however a significant increase in the FWHM of the 2D band is observed wherein it increases from 43.7 cm^{-1} to nearly 51.6 cm^{-1} accompanied by a reduction in the I_{2D}/I_G ratio to 0.49 from 1.03 for pristine FLGs. From the SEM image of Figure 1(d), it can be clearly observed that the organo-silane treatment clearly leads to an increase in the edge thickness of the flakes which thereby leads to the formation of multi-layer graphene like structures. Since the FLG are vertically aligned on a Si-substrate, it is expected that only the top-most surfaces of the FLG would be predominantly accessible to atomic hydrogen/nitrogen/silicon during the functionalization procedure.

XANES and XPS analysis: For graphitic materials in general, the X-ray Absorption near edge structure (XANES) spectra can be divided into three regions characterized by specific resonance energies.[58] The first region of π* resonance appears around 285± 1 eV, the C-H* resonance around 288 ± 1 eV, and a broad region between 290 eV – 315 eV corresponds to σ* resonance. The presence of the π* and C-H* resonances serve as a fingerprint for the existence of sp^2 hybridized C-C bonds and C-H bonds, respectively. Figure 3 shows the C *K*-edge XANES spectra of the FLGs with spectral features at ~285.1 (±1) eV, ~292.6 (±1) eV and ~291.6 (±1) eV; which are attributed to the unoccupied 1s →π*, 1s →σ* and excitonic states transitions, respectively.[58] The peak positions for graphone are similar to that of pristine FLG, but the absorption edges of N-graphene/siliphene are shifted towards higher/lower energy levels that can be seen clearly from the first order derivatives of all the C *K*-edge XANES spectra shown in S1 (Supplementary information). This change in the absorption edge is attributed to the change in the band gap of N-graphene/siliphene due to the structural rearrangement via carbon bonding with nitrogen and silicon, respectively.[59, 60] Apart from the π* and σ* resonance peaks, two other peaks at ~287.4 (±1) eV and ~288.5 (±1) eV are observed and are ascribed as signatures of C-H bonds and interlayer graphite states, respectively (also shown inset below in figure 3). When compared to the pristine FLG spectra, the graphone spectra show an increased intensity of the C-H peak accompanied by a reduction in the interlayer graphite peak intensity. This increase in the C-H peak intensity confirms the formation of sp^3-rich structures having a higher content of C-H bonds. In the case of N-Graphene, the C*K*-edge XANES spectrum shows a strong peak at 0.2 eV below the interlayer graphite peak (marked with a green line bar), which may arise from the contribution of N- and O- related bonds in N-graphene. The Si-functionalized C *K*-edge XANES spectra show that both the π* and σ* peaks are wider and show a downward energy shift which is different from graphone/N-graphene. A similar downward energy shift has also been observed in Si-treated diamond-like carbon thin films[59] indicating the change of band gap of the material. The wide π* region may be double features due to the possibility of the formation of two different kinds of bonds, namely, Si-C(:H) /Si-C(:O) and sp^2 C-C bonds, which were also observed by Terekhov et al. in their XANES study of *a*-$Si_{0.4}C_{0.6}$:H composite materials.[60]

The general line shape of the C *K*-edge XANES spectrum of SiC/β-SiC[60, 61] is clearly very different from that of siliphene, which indicates the absence of SiC segregations in siliphene. The *π** feature becomes wider for siliphene and similar broadening has also been observed in CVD diamond (see reference 5, Figure 6). On comparison with the spectral features of the CVD diamond[60, 61], the siliphene can be concluded to contain an increased number of sp^3-hybridized atoms with diamond-like character. Again, the interlayer graphitic peak is not observed in case of siliphene like graphone/N-graphene, thus, there is a possibility of the

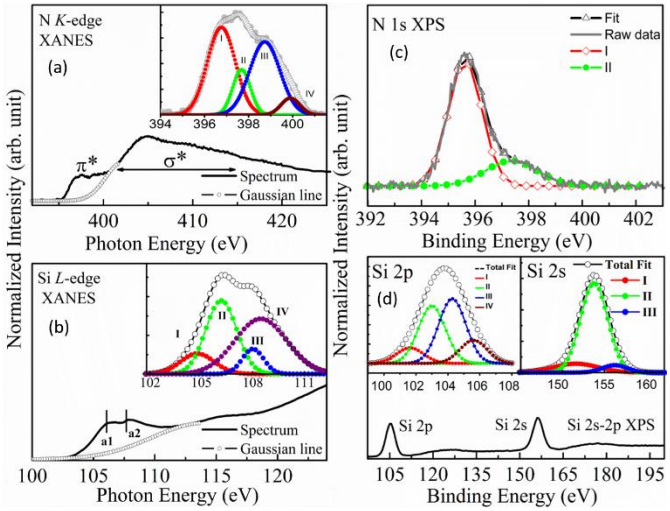

Figure 4. (a) N *K*-edge XANES spectra of N-graphene with its deconvolution in the inset, (b) Si *L*-edge XANES spectra of siliphene with its corresponding deconvolution in the inset, (c) N 1s XPS spectra of N-graphene with its deconvolution and (d) Si 2p-Si 2s XPS spectra of siliphene with their corresponding deconvolution in the inset.

formation of the Si-C(:O) bonding in addition to the Si-C(:H) bonding. Inset above in Figure 3 shows the C 1s core-level XPS spectra. The peak observed at ~285.0 eV for both FLGs and graphone can be assigned as the C-C bond, which is shifted to the higher energy at ~285.2 eV and became broader for siliphene. Pedio et al.[62] studied the dependence of the formation of C_{60} on silicon surfaces on the annealing temperature using C 1s XPS measurements and found that the C-C bond and C-Si bond features are located at 284.2 and 282.6 eV, respectively. In the present case, the spectral features are different and apparently do not have the signature of SiC segregations in C 1s core-level XPS spectra, which further confirms enhanced sp^3 bonding (i.e., diamond and/or diamond-like carbon) rather than sp^2 bonding (like graphite and/or CNTs) and/or C-Si bonding. This result is consistent with those obtained from Raman and XANES measurements. The enhancement of Si-C tetrahedral bonding (sp^3 bonding) and reduction of sp^2 bonding improves the reactivity of siliphene, as the surface atoms with sp^3 bonding have dangling bonds. In the case of N-graphene, the C 1s peak position is shifted to a lower energy level at ~282.1 eV indicating the formation of more graphitic structure and probable with the formation of nitrogen bonding in N-graphene. Moreover for detailed analysis about the presence of nitrogen-bonding and Si-bonding with C in N-graphene/ siliphene, we have also studied the N *K*-edge (Si *L*-edge) XANES and N 1s (Si- 2p-2s) XPS spectra, the results of which are discussed below.

Figure 4 shows the N *K*-edge (Si *L*-edge) XANES and N 1s (Si-2p-2s) XPS spectra of N-graphene/siliphene. The π* region of N *K*-edge XANES spectrum was deconvoluted into three components, while the N1s XPS spectra was deconvoluted into two components using Gaussian lineshapes; which are shown in figure 4(a, c), respectively. The four peaks in the N*K*-edge XANES spectrum are located at ~396.7, 397.7, 398.7 and 399.9 eV which can be attributed to nitrogen in nitride phase, pyridine-like bonding and pyrrole/subsitutional graphite like bonding.[63] Similar peak positions have been observed by Geng et al. in their study of nitrogen doping effects on the structure of graphene. The π* resonance peak at 397.7 eV is attributed to pyridine-like bonding and arises from transitions from the K-shell (N1s) to the unoccupied π* orbital.[64, 65] The two peaks observed in the N 1s XPS spectrum are at ~395.7 and 397.4 eV and can be ascribed to nitride-like species or aromatic N-imines and pyridine like species[66] and is corroborated by N1s XANES spectra. The peak position of the pyridine like species is however 1.0 eV lower to that reported by Liu et al in the case of nitrogen doped graphene oxide.[33] For siliphene, the Si *L*-edge spectrum is composed of four Gaussian peaks at 104.7 (I), 106.2 (II), 108.0 (III) and 108.5 eV (IV). These peaks are mainly Si 2p→3s transition (Peak I and II), split into $L_{2,3}$-peak, and Si 2p→3p/3d transitions (peak III and IV) as observed by Gaultois et al. in $(TiO_2)_x(SiO_2)_{1-x}$ composite[67], Li *et al*. in quartz[68] and Tsai et al. in SiO_2 materials[69]. The curve fitting of the Si 2p XPS was carried out using four Gaussian peaks at 101.6 (I), 103.0 (II), 104.2 (III) and 105.6 eV (IV), corresponding to Si-C, Si-C(:O)/Si-C(:H), Si-O and SiO_x species respectively[35, 70, 71], although we have not observed any prominent Si-C peak in XANES spectrum. The results match very well with those observed for SiC thin films prepared using chemical vapor deposition method.[71] While the Si incorporation occurs in the graphene lattice to form sp^3-hybridized atoms or tetrahedral bonding with diamond-like character; the post functionalisation exposure of the samples to the ambient environment leads to the formation of Si-C(:O)/Si-C(:H) bonding. In Si 2s XPS decomposed into three peaks *viz*. 151.6(I), 153.7(II) and 156.4(III) and ascribed as Si-Si (I) and Si-O (II& III).[70]

Magnetic Measurements: Now, the magnetic properties of the FLG and graphone/N-graphene/siliphene were measured within the range of -2 kOe < H < 2 kOe at temperatures of 300 K and 40 K, respectively. The measured magnetic hysteresis loops are shown in Figure 5, with the N-graphene (Figure 5c) showing the most expressed ferromagnetic behaviour with lowest field hysteretic features (H_r = 40 Oe) and highest saturation moment (Ms = 118.62 x 10^{-4} emu/gm), whereas the siliphene shows highest hysteretic features (H_r = 120.03 Oe) and lowest saturation moment (Ms = 0.11 x 10^{-4} emu/gm). As compared to the pristine FLGs (Ms = 3.47 x 10^{-4} emu/gm), the magnetic moment values of graphone (figure 5b) is higher (Ms = 13.94 x 10^{-4} emu/gm) due to the incorporation of hydrogen in the FLG as observed in C *K*-edge XANES spectrum, resulting in the formation of sp^3 hybridized carbon structure through mono and possible di-hydrogen termination. Similar increase in the magnetic properties of graphene exposed to hydrogen has been reported recently by Herrero et al., wherein they deposited a single hydrogen atom on top of graphene and then utilised scanning tunnelling microscopy to detect magnetism on the sublattice lacking the deposited atom.[72] In the case of siliphene, the spectral feature is entirely different

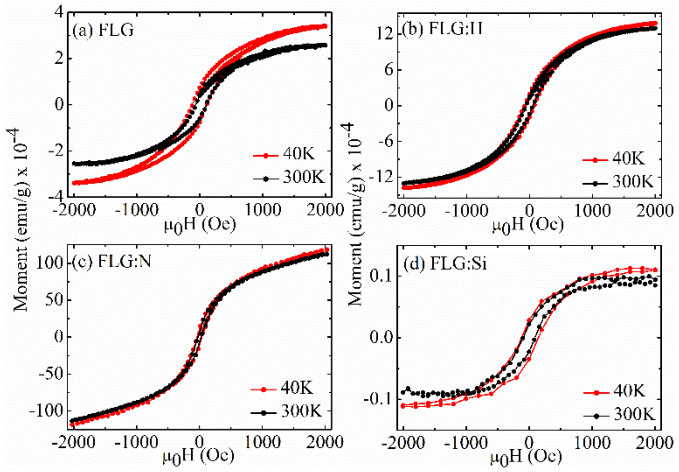

Figure 5. Magnetic hysteresis loops obtained for (a) FLG, (b) Graphone, (c) N-graphene and (d) Siliphene at 300 K and 40 K, respectively.

than graphone/N-graphene and is considered as mixed dia- and ferro-magnetic in nature as shown in S2 (Supplementary information). Due to presence of mixed dia- and ferro-magnetic nature, we have subtracted the diamagnetic background revealing that the saturation magnetic moment is ~ 0.11 x 10^{-4} emu/gm only, significantly lower as compared to graphone/N-graphene and even lower than pristine FLGs (Ms = 3.47 emu/gm) as shown in figure 5(d). As the FLG are free from any catalyst remnants (Supplementary Information, Fig. S3) and detectable foreign magnetic impurities, the observed magnetism can be attributed to the defects and vacancies created during synthesis, and the creation of sp^3 hybridised structures.[73-75] Previously, He et al., reported the magnetisation of the $^{12}C^+$ implanted highly oriented pyrolytic graphite (HOPG) was found to be closely correlated with the density of defects and an almost linear relationship between the ID/IG ratio and saturation magnetisation was observed.[76] As the N-graphene shows the highest I_D/I_G ratio, it is expected and indeed observed that the N-graphene displays highest magnetization value, followed by the graphone.

Even though the nitrogenation[33] and hydrogenation[23, 77] may possibly occur on only the top-most surface layers of the FLG; thereby favouring the higher observed saturation magnetic moment compared to pure FLG; but their inherent mechanisms are different to each other. In the case of hydrogenation, the magnetism is due to the formation of sp^3-rich hybridized structure thereby favouring ferromagnetism, as reported in our earlier work[23] and similar to those reported earlier[78]; whereas, for nitrogenation the magnetism is due to the extra π-electron from nitrogen making the structure electron-rich, thereby, enhancing the magnetic coupling between magnetic moments[33]. In their recent work, Miao et al. observed enhanced ferromagnetism in N-doped graphene with an increase in the saturation magnetisation and coercive field with an increase in the nitrogen content, especially pyrrolic groups of the samples which can induce a net magnetic moment of 0.95 μ_B/N.[79] Based on different hydrogen attachment configurations on graphene, Yazyev et al predicted[80] that the ortho-dimers and para-dimers are nonmagnetic, while single hydrogen attachment (monomer) are magnetic in nature.[80] This may explain why graphone is more magnetic than FLG. Wang et al.[81] proposed long-range coupling of spin units (defects) to be responsible for ferromagnetism in graphone whereas Xie et al.,[82] for partially hydrogenated graphene, have invoked the formation of unpaired electrons in graphene which together with the remnant delocalised π bonding network introduces the observe ferromagnetism. In the case of N-graphene, the Fermi level shifts upwards due to the extra π electron that makes graphene electron-rich.[34] The shift of C *K*-edge and formation of different carbon – nitrogen bonds observed in N *K*-edge XANES spectra clearly indicated the formation of π electron and Fermi level shift. The high value of I_D/I_G ratio of N-graphene also implies the defect rich N-graphene. This result suggested that the magnetic properties of the super lattices were entirely determined by the graphitic region due to the π character of the spin density. Thus, N-doping enhances the direct type of magnetic coupling between the magnetic moments due to the decrease in the distance between the magnetic moments. Moreover, the presence of magnetic exchange or coupling between the localized magnetic moments is a necessary ingredient for the magnetic cooperative behaviour such as ferromagnetic ordering. It is noted that the specific contribution made by each specific type of two N types (pyridine-like and cyanide- like) is complicated, and it is difficult to clarify the specific contribution in N-graphene. Interestingly, the nitrogen doping (N-graphene) increases the magnetization by almost 34 times as compared to pristine FLGs. Similar enhancement of magnetisation (~15 times higher) was also observed by Liu et al.[33] in their study of nitrogen doped GO. So, it is very clear from this study that N-doping result in the increase of the magnetization of FLG and the generation of ferromagnetism. In the case of siliphene, it is observed from the C *K*-edge XANES spectra that the sample contains an increased number of sp^3-hybridized atoms or tetrahedral bonding with diamond-like character with possibility of the formation of the Si-C(:O)/Si-C(:H) bonding. The Si-C/Si-O bonding is observed in the Si *L*-edge XANES as well as the Si *2p-2s* XPS spectrum. As compared to pristine FLG, the band gap of siliphene is enhanced. As pure SiC is a direct band gap semiconductor material, the conduction band bottom and valence band maximum are located at Brillouin Zone Γ-point and have no phenomena of spin polarization; thereby non-defective tetrahedral bonding SiC has no magnetism.[81] Hence, the magnetization is reduced after formation of SiC and SiO in the siliphene structure.

MFM measurements: Further detection of the magnetic domains in the pristine and graphone/N-graphene/siliphene was carried out by magnetic force microscopy (MFM) measurements using low moment magnetic probes with Co/Cr coating. Figures 6 & 7 show the topographic (height), amplitude and phase signals imaged simultaneously for both tapping mode AFM (TM-AFM) and magnetic force microscopy (MFM) mode to assess the correlation of surface features, identify and eliminate possible artifacts and to assess the

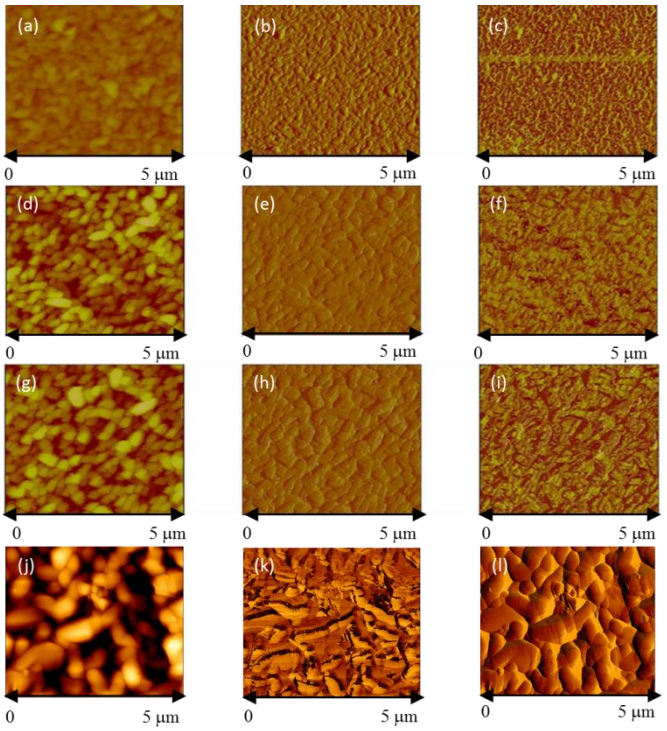

Figure 6. Atomic Force Microscopy (topography, phase, amplitude) images of pristine FLG (a–c), Graphone (d–f), N-graphene (g–i) and Siliphene (j-l).

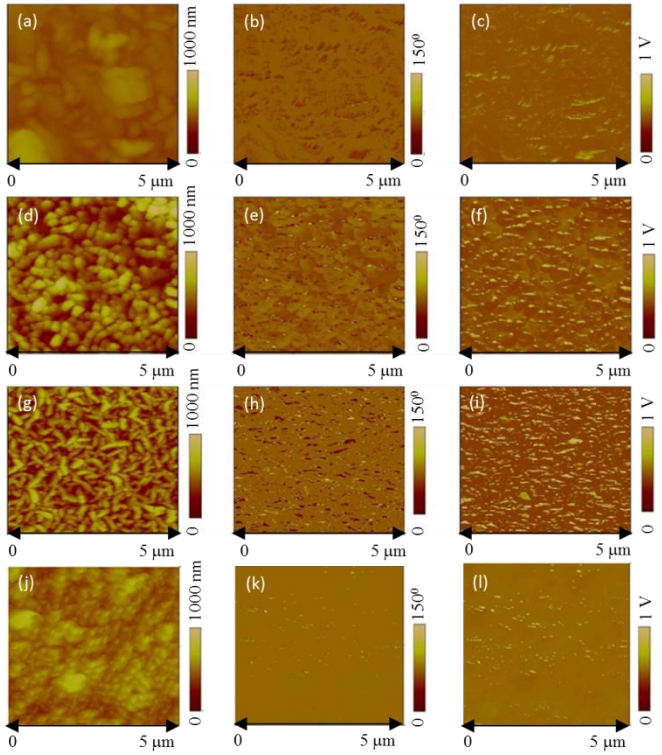

Figure 7. Magnetic Force Microscopy (topography, phase, amplitude) images of pristine FLG (a–c), Graphone (d–f), N-graphene (g–i) and Siliphene (j-l).

effects of functionalization on magnetization. The magnetized Co/Cr coated probe interacts with magnetic field gradients generated by magnetic domains within the prepared FLGs resulting in changes in the phase and amplitude of the oscillating cantilever. To assess the correlation of surface features and the effects of magnetization, the topographic (height), amplitude and phase signals were imaged simultaneously for both conventional topographical imaging and magnetic measurements. MFM data were acquired while maintaining a constant "lift scan height" of ~10 nm above the topography (height) data to reduce coupling between Van der Waals and magnetic forces and also to demonstrate the field strength generated by the magnetic domains. In "lift-scan" mode, the topography is measured in the dynamic amplitude modulation mode after which the tip is then moved at a constant distance above the surface during which the magnetic component of the data is recorded.[23] In theory, the topographic contributions should get eliminated in the second image. Comparing the AFM scans of the samples with the MFM scans, while no significant changes are observed in the topographic signal; significant differences are observed in the phase and amplitude scans. For the conventional AFM scans, the phase signal is essentially a map of how the phase of the cantilever oscillation is affected by its interaction with the sample surface and is affected highly by topography among other factors such as chemical nature, relative hardness/softness of the sample. Since the MFM signal represents the phase shift between the probe oscillation and the driving signal due to magnetic force acting on the tip, therefore by visualising/measuring the changes occurring in the amplitude and phase images, the existence of magnetic domains in the samples can be ascertained.

For a true quantitative interpretation of the MFM images, it is necessary to have precise knowledge of the geometry, magnetic properties of the tip and the tip-sample interactions in order to express the force acting on the tip, which has only been achieved in special cases.[83, 84] Nevertheless, a qualitative analysis can be carried out by considering the phase and amplitude changes observed in the MFM images (Fig. 7). It should be noted that an attractive interaction between the between the tip and the sample leads to a negative phase shift (dark contrast), while a repulsive interaction will lead to a positive phase shift (bright contrast). In fact, the MFM phase and amplitude images show a very good correlation in the formation of the magnetic domains. For all the FLG samples, the magnetic domains appear as dark and bright-localized regions in the phase and amplitude images respectively. Considering Figs. 7(c, f, i, l) representing amplitude images of pristine, graphone, N-graphene and siliphene, it can be clearly observed that the magnetic domains in the graphone/N-graphene are more localized than in the case of pristine FLG and indeed siliphene. Especially, in the case of siliphene, the lack of contrast in phase and amplitude images with respect to pristine FLGs showed a reduction in the presence of magnetic domains which essentially leads to the lowering of the magnetic response from the sample. A simple visual scaling of MFM phase data suggests that the siliphene has the weakest magnetization, whereas the N-graphene/graphone the strongest magnetization effect, which is consistent with the M-H magnetization results, described above.

Effect of functionalisation: The application of graphene is limited in spintronics devices due to its semi-metallic behaviour. Hence, opening of the zero bandgap of graphene to semiconducting region is highly necessary with the fabrication of p-type and n-type semiconductors. For any type of spintronics device application, the materials should have semiconducting and enhanced magnetic properties. Hence, it is necessary to choose a particular element to functionalize the graphene to induce semi-metallic behaviour to semiconducting behaviour without compromising beneficial magnetic properties so that the materials can withstand the applications as observed in diluted magnetic semiconductor (DMSs). It is well known that graphene possesses very profitable magnetic behaviour due to its sp^2 hybridization bonding between carbons. The magnetic hysteresis of the samples show a form of ferromagnetic field response i.e. induced ferromagnetism behaviour both at low temperature and room temperature in all pristine and functionalized systems [Fig. 5(a-d)] wherein an increase in the saturation magnetization is observed; which is a natural consequence of quenching of thermal energy from the magnetic spin system upon lowering the temperature. However, the magnetic moment at low temperature is higher than the room temperature. This indicates the defective structure associated in the graphene is due to the disruption of the sp^2 hybridization of the carbon atoms. It is noteworthy that graphene usually shows p-type conduction due to the presence of adsorbed oxygen or water molecules on the graphene surface. Hence, graphene functionalized with H, N and Si is taken in consideration to form n-type semiconductor and to observe how magnetic behavior changes with respect to the functionalized elements.

Hydrogen incorporation of graphene increases the sp^3 hybridization but bonding with carbon reduces the defect present in the pristine graphene sheet. In this case, there is not much variation in the saturation magnetization value at low and room temperature as shown in Fig. 5(b). The saturation magnetization value is increased to four times the saturation value of pristine graphene. Even the magnetic behaviour is enhanced by the functionalization of H, but it is not considered suitable materials to use in field effect transistor, memory storage devices and other spintronics devices due to small opening of the bandgap (i.e. 0.27 eV).[85] However, nitrogen doped/functionalized graphene sheet (N-graphene) shows significant enhancement of magnetism as observed and shown in Fig. 5(c). It was reported earlier by the authors and many other groups[33] that nitrogen has a strong affinity towards carbon and forms sp^2 like hybridized bonds. Not only does the sp^2 hybridization bonding increases but as well it increases the percentage of unpaired electrons due to its electronic structure of $1s^2 2s^2 2p^3$. As Nitrogen's p orbital is half filled, its bonding with carbon is always left with one unpaired electrons. This unpaired electron is the mechanism of enhancing the saturation magnetization in a large value i.e. 34 times higher than the saturation magnetization value of graphene. It is reported that the bandgap of N-functionalized graphene is almost 1.23 eV[85] and the nature of semiconductor is of n-type. However, maximum opening of bandgap can occur up to 2.01 eV depending upon the percentage of Si in graphene[86] and the structure is popularly known as siliphene. The M-H loop measurements for Si functionalized graphene are plotted in Fig. 5(d). The as measured data demonstrates magnification values that are extremely small, *viz* more than one order of magnitude smaller than the other materials studied in this report, hence a diamagnetic signal was detected especially at higher fields in the form dM/dH <0. It is observed that the saturation magnetisation was decreased by 30 times in comparison to the pristine graphene.

Table 1: Magnetic properties of the pristine and plasma treated graphene samples at 40 K and 300 K

Sample/ Temperature	H_c (Coercivity) (Oe)	M_s (Saturation magnetisation) (emu/gm)	M_r (Remnant magnetisation) (emu/gm)
Pristine FLG			
40K	112.37	3.47×10^{-4}	0.52×10^{-4}
300K	62.98	2.60×10^{-4}	0.42×10^{-4}
Graphone			
40K	76.19	13.94×10^{-4}	1.91×10^{-4}
300K	52.88	12.91×10^{-4}	1.28×10^{-4}
N-Graphene			
40K	40.00	118.62×10^{-4}	9.74×10^{-4}
300K	25.42	111.91×10^{-4}	6.04×10^{-4}
Siliphene			
40K	120.03	0.11×10^{-4}	0.03×10^{-4}
300K	94.75	0.09×10^{-4}	0.02×10^{-4}

This reduction in the magnetic behaviour suggests that Si incorporation in to graphene forms a strong interaction between Si-C which are tetrahedral bonded at the cost of sp^2 hybridization present in graphene. However, during synthesis and subsequent exposure to the ambient environment, the contamination of oxygen occurs with Si and forms a bond Si-O and as a consequence, it reacts with carbon contain graphene and forms clusters like Si-O-C (defect structure). This is the mechanism behind the observation of ferromagnetic behaviour. Here, the saturation magnetization does not vary a lot at 40 K and 300 K, which represents that there is a structural ordering between Si and C. It is reported in literature that the incorporation of Si in graphene transforms the semi-metallic magnetic graphene to semiconducting magnetic graphene which has a large area of application field emission transistors and in spintronics devices. In this case, Si is a good candidate to provide both semiconducting as well as magnetic properties in graphene if Si can be doped in a controlled way. As in our study, Si incorporation reduces the magnetization value severely but on the other hand opens a new path for the application in spintronics devices.

To have a comparative view on saturation magnetization, remnant magnetization and coercivity of H, N and Si functionalized graphene, the analysis has been presented in Table 1. It seems that the coercivity values of siliphene are highest and the corresponding saturation magnetisation are lowest compared to graphone/N-graphene. Similar behaviour

has been observed in graphene oxide and reduced graphene oxides and has been attributed to an increase in the structural disorder leading to an increase in the anisotropy energy density which leads to an increase in the coercivity.[87] The siliphene is amenable to high coercivity ferromagnetic materials and are known as magnetically hard materials; whereas the N-graphene shows low coercivity and are termed to be magnetically soft materials. However, the coercivity values of graphone/N-graphene/siliphene are almost similar at 40 K and 300 K respectively, indicating that all the elements are homogenously distributed throughout the graphene matrix and have no thermal evolution of the magnetic species or the coupling between them. This homogeneous arrangement of functionalized elements in graphene represents the synthesis technique adopted is a unique one for the fabrication of junction devices and field effect transistors as desired for semiconductor applications.

Conclusions

In summary, we have observed the room-temperature ferromagnetism of different FLG materials functionalized with hydrogen/nitrogen/silicon species. The ferromagnetism may originate in the long-range coupling of spin units existing as defects in graphene sheets, which are generated during functionalization process. But more direct evidence is needed for a quantitative assessment. The intrinsic room-temperature ferromagnetic character of the materials, but without the constraint of spontaneous magnetization, combined with its semi-conductivity and functionalization capability, should have wide-reaching implications in material science, and these collective properties could make graphene-based materials a competent choice for many important device applications, including spintronics, magneto-resistance, magnetic memory devices, and so on. Our results may also prompt more thorough and quantitative assessment of room-temperature ferromagnetism of pure FLG, including graphone/N-graphene/siliphene. Moreover, we believe that the non-uniform distribution of the hydrogen, nitrogen and silicon atoms over the FLG plane may also produce ferromagnetic clustering or spin-glass dynamics with attributes that would also deserve further in-depth studies beyond our present state of magnetization.

Acknowledgements

The author S.C.R. acknowledges to National Research Foundation, South Africa for financial support. AMS thanks the SA-NRF (93549), the FRC and URC of UJ for financial assistance. D. Britz is thanked for his assistance with the magnetic measurements.

Notes and references

1 K. S. Novoselov, A. K. Geim, S. V. Morozov, D. Jiang, Y. Zhang, S. A. Dubonos, I. V. Grigorieva and A. A. Firsov, *Science,* 2004, **306**, 666-669.
2 A. K. Geim, and K. S. Novoselov, *Nat. Mater*. 2007, **6**, 183-191.
3 R.K. Layek, and A. K. Nandi, *Polymer* 2013, **54**, 5087-5103.
4 E. W. Hill, A. Vijayaragahvan, and K. S. Novoselov, *IEEE Sensors J*, 2011, **11(12)**, 3161-3170.
5 W. Choi, I. Lahiri, R. Seelaboyina, and Y. S. Kang, *Crit Rev Solid State Mater Sci,* 2010, **35**, 52-71.
6 Y. Si and E. T. Samulski, *Nano Lett.* 2008, **8(6)**, 1679-1682.
7 V. Singh, D. Joung, L. Zhai, S. Das, S. I. Khondaker and S. Seal, *Prog Mater Sci*. 2011, **56(8)**, 1178-1271.
8 N. A. H. Castro, F. Guinea, N. M. R. Peres, K. S. Novoselov and A. K. Geim, *Rev. Mod. Phys.* Phys. 2009, **81**, 109.
9 S. Basu and P. Bhattacharyya, *Sens Actuators* B, 2012, **173**, 1-21.
10 D. A. L. Gomez, Y. Zhang, C. W. Schlenker, K. Ryu, M. E. Thompson and C. Zhou, *ACS Nano* 2010, **4(5)**, 2865-2873.
11 Y. Zhu, S. Murali, W. Cai, X. Li, J. W. Suk, J. R. Potts and R. S. Ruoff, *Adv Mater***.** 2010, **22(35)**, 3906-3924.
12 M. J. Allen, V. C. Tung, L. Gomez, Z. Xu, L. M. Chen, K. S. Nelson, C. Zhou, R. B. Kaner and Y. Yang, *Adv Mater* 2009, **21**, 2098-2102.
13 R. V. Gorbachev, A. S. Mayorov, A. K. Savchenko, D. W. Horsell and F. Guinea, *Nano Lett*. 2008, **8(7)**, 1995-1999.
14 M. Dragoman, and D. Dragoman, *Prog Quantum Electron*. 2009, **33(6)**, 165-214.
15 Y. Zhao, X. G. Li, X. Zhou and Y. N. Zhang, *Sensor Actuat. B-Chem.*, 2016, **231**, 324-340.
16 R. K. Upadhyay, N. Soin, S. S. Roy, *RSC Adv.,* 2014, **4(8),** 3823-3851.
17 F. Schwierz, *Nature Nanotech*. 2010, **5**, 487-496.
18 D. W. Boukhvalov, M. I. Katsnelson, and A. I. Lichtenstein, *Phys Rev B* 2008, **77**, 035427.
19 G. Mittal, V. Dhand, K. Y. Rhee, S. J. Park and W. R. Lee, *J. Ind. Eng. Chem.,* 2015, **21**, 11-25.
20 L. Li, R. Qin, H. Li, L. Yu, Q. Liu, G. Luo, Z. Gao and J. Lu, *ACS Nano* 2011, **5(4)**, 2601-2610.
21 J. Zhou, Q. Wang, Q. Sun, X. S. Chen, Y. Kawazoe and P. Jena, *Nano Lett*. 2009, **9(11)**, 3867-3870.
22 N. Lu, Z. Li and J. Yang, *J. Phys Chem C* 2009, **113(38)**, 16741-16746.
23 S. C. Ray, N. Soin, T. Magkato, C. H. Chuang, W. F. Pong, S. S. Roy, S. K. Ghosh, A. M. Strydom and J. A. McLaughlin, *Sci. Rep*. 2014, **4**, 3862.
24 D. C. Elias, R. R. Nair, T. M. G. Mohiuddin, S. V. Morozov, P. Blake, M. P. Halsall, A. C. Ferrari, D. W. Boukhvalov, M. I. Katsnelson, A. K. Geim and K. S. Novoselov, *Science* 2009, **323**, 610-613.
25 X. D. Wen, T. Yang, R. Hoffman, N. W. Ashcroft, R. L Martin, S. P. Rudin and J. X. Zhu, *ACS Nano*, 2012, **6(8)**, 7142-7150.
26 J. D. Jones, K. K. Mahajan, W. H. Williams, P. A. Ecton, Y. Mo and J. M. Perez, *Carbon,* 2010, **48**, 2335-2340.
27 S. U. Lee, R. V. Belosludov, H. Mizuseki and Y. Kawazoe, *Small* 2009, **5(15)**, 1769-1775.
28 Y. F. Li, Z. Zhou, P. W. Shen, and Z. F. Chen, *ACS Nano* 2009, **3(7)**, 1952-1958.
29 Y. C. Ma, A. S. Foster, A. V. Krasheninnikov, and R. M. Nieminen, *Phys. Rev. B* 2005, **72**, 205416.
30 C. C. Ma, X. H. Shao and D. P. Cao, *J. Mater. Chem.* 2012, **22**, 8911-8915.
31 Y. Zhang, S. Talapatra, S. Kar, R. Vajtai, S. K. Nayak and P. M. Ajayan, *Phys. Rev. Lett.* 2007, **99**, 107201.
32 J. Y. Dai and J. M. Yuan, *Phys. Rev. B* 2010, **81**, 165414.
33 Y. Liu, N. Tang, X. Wan, Q. Feng, M. Li, Q. Xu, F. Liu and Y. Du, *Sci. Rep*. 2013, **3**, 2566.
34 S. Jalili and R. Vaziri, *Mol. Phys*. 2011, **109**, 687-694.
35 C. W. Pao, S. C. Ray, H. M. Tsai, Y. S. Chen, H. C. Chen, I. N. Lin, W. F. Pong, J. W. Chiou, N. G. Shang and P.

Papakonstantinou, *J. Phys. Chem. C* 2010, **114(18)**, 8161-8166.
36 P. A. Denis, *Chem. Phys. Lett*. 2010, **492**, 251-257.
37 K. Ando, *Science 2006,* **312**, 1883-1885.
38 Y. F. Wang, S. B. Singh, M. V. Limaye, Y. C. Shao, S. H. Hsieh, L. Y. Chen, H. C. Hsueh, H. T. Wang, J. W. Chiou, Y. C. Yeh, C. W. Chen, C. H. Chen, S. C. Ray, J. Wang, W. F. Pong, Y. Takagi, T. Ohigashi, T. Yokoyama and N. Kosugi, *Sci. Rep*. 2015, **5**, 15439.
39 S. B. Fagan, R. Mota, R. J. Baierle, A. J. R. daSilva and A. Fazzio, *Diam. Relat. Mater.* 2003, **12**, 861-863.
40 J. W. Chiou, S. C. Ray, S. I. Peng, C. H. Chuang, B. Y. Wang, H. M. Tsai, C. W. Pao, H. J. Lin, Y. C. Shao, Y. F. Wang and S. C. Chen, *J. Phys. Chem. C* 2012, **116(30)**, 16251-16258.
41 S. C. Ray, U. Palnitkar, C. W. Pao, H. M. Tsai, W. F. Pong, I. N. Lin, P. Papakonstantinou, A. Ganguly, L. C. Chen, and K. H. Chen, *J. Appl. Phys.* 2008, **104**, 063710.
42 S. C. Ray, W. Mbiombi and P. Papakonstantinou, *Curr. Appl. Phys.* 2014, **14**, 1845-1848.
43 A. C. Ferrari, J. C. Meyer, V. Scardaci, C. Casiraghi, M. Lazzeri, F. Mauri, S. Piscanec, D. Jiang, K. S. Novoselov, S. Roth and A. K. Geim, *Phys. Rev. Lett.* 2006, **97**, 187401.
44 A. C. Ferrari, *Solid State Commun*. 2007, **143**, 47-57.
45 F. Tuinstra and J. L. Koenig, *J. Chem. Phys*. 1970, **53**, 1126.
46 A. C. Ferrari and J. Robertson, *Phys. Rev. B* 2000, **61**, 14095.
47 W. Wu, Q. Yu, P. Peng, Z. Liu, J. Bao and S. S. Pei, *Nanotechnology* 2012, **23**, 035603.
48 N. Soin, S. S. Roy, S. Roy, K. S. Hazra, D. S. Misra, T. H. Lim, C. J. D. Hetherington and J. A. McLaughlin, *J. Phys. Chem. C* 2011, **115**, 5366-5372.
49 N. Soin, S. S. Roy, C. OKane, J. A. D. McLaughlin, T. H. Lim and C. J. D. Hetherington, *Cryst. Eng. Comm* 2011, **13**, 312-318.
50 K. S. Subrahmanyam, L. S. Panchakarla, A. Govindaraj and C. N. R. Rao, *J. Phys. Chem. C*, 2009, **113(11)**, 4257-4259.
51 S. Pisana, M. Lazzeri, C. Casiraghi, K. S. Novoselov, A. K. Geim, A. C. Ferrari and F. Mauri, *Nat. Mat.* 2007, **6(3),** 198-201.
52 J. Yan, Y. Zhang, P. Kim and A. Pinczuk, *Phys. Rev. Lett*, 2007, ***98*(16),** 166802.
53 Y. Y. Wang, Z. H. Ni, T. Yu, Z. X. Shen, H. M. Wang, Y. H. Wu, W. Chen and A. T. S. Wee, *J. Phys. Chem. C* 2008, **112(29)**, 10637-10640.
54 D. Graf, F. Molitor, K. Ensslin, C. Stampfer, A. Jungen, C. Hierold and L. Wirtz, *Nano Lett*. 2007, **7(2)**, 238-242.
55 S. Ryu, M. Y. Han, J. Maultzsch, T. F. Heinz, P. Kim, M. L. Steigerwald and L. E. S. Brus, *Nano Lett.* 2008, **8(12)**, 4597-4602.
56 L. Xie, L. Jiao and H. Dai, *J. Am. Chem. Soc.,* 2010, **132(42),** 14751-14753.
57 A. Eckmann, A. Felten, A. Mishchenko, L. Britnell, R. Krupke, K. S. Novoselov and C. Casiraghi, *Nano Lett.*, 2012, ***12*(8),** 3925-3930.
58 S. C. Ray, J. W. Chiou, W. F. Pong, and M. H. Tsai, *Crit. Rev. Solid State Mater. Sci.,* 2006, **31(4)**, 91-110.
59 S. C. Ray, C. W. Bao, H.M. Tsai, J.W. Chiou, J.C. Jan, K.K. Kumar, W. F. Pong, M. H. Tsai, W. J. Wang, C. J. Hsu, and T. I. T. Okpalugo, *Appl. Phys. Lett.* 2004, **85**, 4022-4024.
60 V. A. Terekhov, E. I. Terukov, I. N. Trapeznikova, M. Kashkarov, O. V. Kurilo, S. Y. Turishchev, A. B. Golodenko, and E. P. Domashevskaya, *Semiconductors,* 2005*,* **39(7)**, 830-834.
61 Y.K. Chang, H.H. Hsieh, W. F. Pong, M. H. Tsai, K. H. Lee, T. E. Dann, F. Z. Chien, P. K. Tseng, K. L. Tsang, W. K. Su and L. C. Chen, *Phys. Rev. B* 1998*,* **58**, 9018.
62 M. Pedio, F. Borgatti, A. Giglia, N. Mahne, S. Nannarone, S. Giovannini, C. Cepek, E. Magnano, G. Bertoni, E. Spiller and M. Sancrotti, *Physica Scripta*. 2005, **T115**, 695-698.
63 D. Geng, S. Yang, Y. Zhang, J. Yang, J. Liu, R. Li, T. K. Sham, X. Sun, S. Ye and S. Knights, *Appl. Surf. Sci.*, 2011, ***257*(21),** 9193-9198.
64 S. C. Ray, C. W. Pao, J. W. Chiou, H. M. Tsai, J. C. Jan, W. F. Pong, R. McCann, S. S. Roy, P. Papakonstantinou, and J. A. McLaughlin, *J. Appl. Phys.* 2005, **98**, 033708.
65 R. Gago, I. Jiménez, J. Neidhardt, B. Abendroth, I. Caretti, L. Hultman and W. Möller, *Phy. Rev. B* 2005, **71**, 125414.
66 H. Dong, C. Liu, H. Ye, L. Hu, B. Fugetsu, W. Dai, Y. Cao, X. Qi, H. Lu and X. Zhang, *Sci. Rep.,* 2015, **5,** 17542.
67 M. W. Gaultois and A. P. Grosvenor, *J. Mater. Chem*., 2011, **21**, 1829-1826.
68 D. Li, G. M. Bancroft, M. Kasrai, M. E. Fleet, X. H. Feng, K. H. Tan and B. X. Yang, *Solid State Comm*. 1993, **87**, 613.
69 H. M. Tsai, S. C. Ray, C. W. Pao, J. W. Chiou, C. L. Huang, C. H. Du, W. F. Pong, M. H. Tsai, A. Fukano and H. Oyanagi, *J. Appl. Phys.* 2008, **103**, 013704.
70 A. Avila, I. Montero, L. Galan, J. M. Ripalda and R. Levy, *J. Appl. Phys.*, 2001, ***89*(1),** 212-216.
71 H. Kim, M. Seo, M. H. Park and J. Cho, *Angew. Chem. Int. Ed.,* 2010, ***49*(12),** 2146-2149.
72 H. González-Herrero, J. M. Gómez-Rodríguez, P. Mallet, M. Moaied, J. J. Palacios, C. Salgado, M. M. Ugeda, J. Y. Veuillen, F. Yndurain and I. Brihuega, *Science* 2016, **352(6284)**, 437-441.
73 H. R. Matte, K. S. Subrahmanyam, and C. N. R. Rao, *J. Phys. Chem. C* 2009, **113(23)**, 9982-9985.
74 H. X. Yang, M. Chshiev, D. W. Boukhvalov, X. Waintal and S. Roche, *Phys. Rev. B* 2011,**84**, 214404.
75 C. S. Rout, A. Kumar, N. Kumar, A. Sundaresan and T. S. Fisher, *Nanoscale,* 2011, **3(3)**, 900-903.
76 Z. He, X. Yang, H. Xia, X. Zhou, M. Zhao, Y. Song and T. Wang, *Carbon*, 2011, **49(6),** 1931-1938.
77 J. S. Bunch, S. S. Verbridge, J. S. Alden, A. M. Van Der Zande, J. M. Parpia, H. G. Craighead and P. L. McEuen, *Nano lett.* 2008, **8(8)**, 2458-2462.
78 G. Ning, C. Xu, L. Hao, O. Kazakova, Z. Fan, H. Wang, K. Wang, J. Gao, W. Qian and F. Wei, *Carbon* 2013, **51**, 390-396.
79 Q. Miao, L. Wang, Z. Liu, B. Wei, F. Xu and W. Fei, *Sci. Rep.* 2016, **6**, 21832.
80 O. V. Yazyev and L. Helm, *Phys. Rev. B* 2007, **75**, 25408.
81 Y. Wang, Y. Huang, Y. Song, X. Zhang, Y. Ma, J. Liang and Y. Chen, *Nano Lett.* 2009, **9**, 220-224.
82 L. Xie, X. Wang, J. Lu, Z. Ni, Z. Luo, H. Mao, R. Wang, Y. Wang, H. Huang, D. Qi and R. Liu, *Appl. Phys. Lett.* 2011, **98**, 193113.
83 J. Červenka, M. I. Katsnelson and C. F. J. Flipse, *Nat. Phys.*, 2009, ***5*(11),** 840-844.
84 W. K. Lee, K. E. Whitener, J. T. Robinson and P. E. Sheehan, *Adv. Mater.*, **27(10),** 2015, 1774-1778.
85 R. Lv and M. Terrones, *Mater. Lett.* 2012, **78**, 209-218.
86 M. S. S. Azadeh, A. Kokabi, M. Hosseini and M. Fardmanesh, *Micro Nano Lett.*, 2011, **6,** 582-585.
87 K. Bagani, A. Bhattacharya, J. Kaur, A. R. Chowdhury, B. Ghosh, M. Sardar and S. Banerjee, *J. Appl. Phys.* 2014, **115**, 023902.
88 N. Soin, S. S. Roy, S. K. Mitra, T. Thundat and J. A. McLaughlin, *J. Mater. Chem*. 2012, **22**, 14944-14950.
89 N. Soin, S. S. Roy, S. Sharma, T. Thundat, and J. A. McLaughlin, *J. Solid State Electrochem.* 2013, **17**, 2139-2149.
90 N. G. Shang, P. Papakonstantinou, M. McMullan, M. Chu, A. Stamboulis, A. Potenza, S. S. Dhesi and H. Marchetto, *Adv. Funct. Mater.* 2008, **18**, 3506-3514.